

Dose distribution in boron neutron capture therapy for the treatment of brain cancer



Leandro O. Pereira^{a,*}, Renato P. Freitas^a, Douglas S. Ferreira^a, Valter S. Felix^a, Elicardo A.S. Gonçalves^a, André R. Pimenta^a, Rafael de Sousa Dutra^a, Ademir Xavier da Silva^b

^a Laboratório de Instrumentação e Simulação Computacional, LISCOMP/IFRJ-CPAR, 26600-000, Paracambi, Brazil

^b Programa de Engenharia Nuclear/COPPE Departamento de Engenharia Nuclear/Escola Politécnica Universidade Federal do Rio de Janeiro, Caixa Postal 68509, CEP 21941-972, Rio de Janeiro, Brazil

ARTICLE INFO

Keywords:

BNCT treatment
MCNP
Epithermal neutron

ABSTRACT

This work presents a study of the influence of the field size of an epithermal neutron beam on the dose distribution in treatments with boron neutron capture therapy using an anthropomorphic voxel-based simulator. To calculate the doses in the tissues and organs of the head, the Monte Carlo N-Particle radiation transport code is used. The results suggest the possibility of using a beam of 6 cm in diameter for the treatment of tumours in the frontal lobe and parietal regions. With a beam of 10 cm in diameter, we could treat tumours located in the frontal lobe, parietal lobe and thalamus. The work also shows that the contribution of the secondary components (gamma rays, fast and thermal neutrons) in the calculation of the total dose can result in up to 15% of the dose in the tumour tissue, 68% of the dose in the healthy brain tissue and 87% of the dose in the non-cephalic regions.

1. Introduction

The application of neutrons in cancer therapy has been a target of clinical and scientific interest since its discovery by Chadwick in 1932 (Chadwick, 1932). Boron neutron capture therapy (BNCT) is a type of radiation therapy for cancer treatment, with its success dependent on the deposition of boron (^{10}B) in tumour cells, followed by irradiation with neutrons, resulting in the production of ionising particles that cause the death of cancer cells.

This therapy is currently used for the treatment of brain tumours multiform glioblastoma (GBM) and skin, among others (Barth, 2005; Faghihi and Khalili, 2013; Farhad Masoudi et al., 2018; Nedunchezian, 2016). In BNCT, a selective delivery agent (protein compound) is used to deposit ^{10}B into cancer cells. The nuclear reaction ($^{10}\text{B} (n, \alpha) ^7\text{Li}$) produced when ^{10}B captures a neutron with energy of the order of 0.025 eV, known as a thermal neutron, releases two short-range fragments in the tissue, of the order of 9 μm for α particles and 5 μm for ^7Li . On this basis, they release their energy inside the cancer cells. Treatment of high-grade astrocytomas is one of the main fields of the action of BNCT. These tumours comprise $\sim 40\%$ of all brain tumours and cause large changes in normal cells (Rogus, 1994; Rogus et al., 1994). GBM is considered an infiltrating malignant neoplasm (reaching depths of up to 8 cm in the brain) that is unpredictable and

uncontrollable, but unable to promote metastasis outside the brain. Topographically, GBM predominates in the supratentorial region, more frequently in the temporal (32%), frontal (31%), fronto-parietal (11%), parietal (10%), temporo-parietal (7%) and occipito-parietals (5%) (Faghihi and Khalili, 2013).

One of the problems of the BNCT technique is the lack of information on dose values in adjacent normal tissue and other radiosensitive tissues of the head and neck region. Since in radiotherapy procedures it is not feasible to perform live dose measurements in the organs, it is necessary to use other more practical methods to estimate the doses absorbed in the patient's organs.

This work aims to investigate the influence of the field size of an idealised beam of neutrons on the dose distribution in treatments with BNCT. In order to achieve this objective, the Monte Carlo N-Particle (MCNP) radiation transport code, a voxel-based head and neck simulator, was used to calculate the doses in the tissues and organs of the head and neck, with analysis of the contributions of the secondary components (secondary gamma rays and fast and thermal neutrons).

* Corresponding author.

E-mail address: leandro.pereira@ifrj.edu.br (L.O. Pereira).

2. Materials and methods

2.1. BNCT

In BNCT, ^{10}B has usually been the chosen isotope because it is stable and presents a high section of capture microscopic shock ($\sigma = 3838 \text{ b}$) for neutrons with an energy of 0.025 eV (Rose, 1991). The total energy released in reaction $^{10}\text{B} (n, \alpha) ^7\text{Li}$ is 2.79 MeV. In 94% of the nuclear reactions, a gamma ray of 0.48 MeV is released. The kinetic energy of the particles is mostly transferred, i.e., 2.31 MeV, to the tumour tissue. However, 6% of reaction $^{10}\text{B} (n, \alpha) ^7\text{Li}$ decays directly to the ground state. To enable nuclear reactions, a non-toxic, ^{10}B atom (brain boron loading) brain tissue binding compound is introduced into the patient by intravenous infusion. Because of the higher metabolic activity of the tumour in relation to the healthy tissue, the concentration of ^{10}B in the tissue/tumour ratio reaches a differential of 1/3 to 1/4, since the cells of the tumour tissue need amino acids for the synthesis of proteins and the generation of new membranes (Bisceglie et al., 2000; Sousa, 2003).

A time interval after the boron atoms preferentially concentrate on the tumour cells, the tumour region is irradiated with a predominantly epithermal neutron beam (Bisceglie et al., 2000; Torres-Sánchez et al., 2019). These neutrons are thermalised in the tissue at energies of the order of 0.0253 eV and are then captured by the ^{10}B atoms, generating reactions that produce doses below the acceptable maximum limits in adjacent healthy tissue. The effectiveness of the treatment is conditioned to the biochemical capacity of the boron compound to concentrate, preferably, on tumour tissue, and a sufficient thermal neutron fluence in the tumour region, so that the neutron capture reaction occurs in the required amount. The preferential accumulation of the boron compound in the cells of the tumour tissue promotes a growth in the amount of the products of reaction $^{10}\text{B} (n, \alpha) ^7\text{Li}$, which release their energy with microscopic selectivity in the region of interest.

The biological response to ionising radiation also depends on the type of radiation and is characterised by the relative biological efficiency (RBE). The RBE is valid only when it is possible to define the amount absorbed dose. For the boron dose (due to reaction $^{10}\text{B} (n, \alpha) ^7\text{Li}$), the absorbed dose concept does not apply because of the non-homogeneous distribution of the boronated compound and also because of the short path length of the α -particles and ^7Li . Therefore, the RBE cannot be defined, and it is also not possible to determine the biological weight factor of a nonhomogeneous distribution of boron atoms. Only the product of these components, the RBE and boron atom distribution, can be determined for a given tissue under experimental conditions. This product is commonly referred to as the compound factor (CF) (IAEA-TECDOC-1223, 2001). The total dose in treatments with BNCT (D_{BNCT}) can then be defined as the sum of the different dose contributions, multiplied by their respective biological weight factors according to Eq. (1) (IAEA-TECDOC-1223, 2001).

$$D_{\text{BNCT}} = W_{\gamma} \cdot D_{\gamma} + W_{\text{FE}} \cdot D_{\text{FE}} + W_{\text{T}} \cdot D_{\text{T}} + W_{\text{CF}} \cdot D_{\text{B}} \quad (1)$$

where W_{γ} , W_{FE} , W_{T} and W_{CF} are the biological weights of gamma, fast neutron and epithermal, thermal neutrons and boron components, respectively. The values of the biological weight factors for the major dose components in BNCT (Palmer et al., 2002) are shown in Table 1.

Table 1
Biological weight factors for the major dose components in BNCT (Palmer et al., 2002).

Factors	w_{γ}	w_{FE}	w_{T}	w_{CF}
Tumour	0.5	3.2	3.2	3.8
Healthy tissues	0.5	3.2	3.2	1.3

2.2. MCNP

Developed at the Los Alamos National Laboratory, USA, MCNP (MCNP – A General Monte Carlo N-Particle Transport Code, Version 5, Volume I: Overview and Theory, LA-UR-03-1987, 2003). is a general purpose code based on the Monte Carlo method. The technique consists of following each particle from its “birth” to its “death” (escape, absorption and so on). The process is based on the selection of random numbers for the computation of the particle transport that we intend to “follow”.

To obtain the results, we used the commands (TALLY F4) that provide the mean particle flow in a given volume cell and the command (DE/DF) that calculates the rate of arbitrary nuclear reactions, allowing for the calculation of the corresponding kerma for each specified material. Further information can be found in the code manual (MCNP – A General Monte Carlo N-Particle Transport Code, Version 5, Volume I: Overview and Theory, LA-UR-03-1987, 2003).

The MCNP code simulates neutron fluids emitted by the source. Thus, all doses are calculated in terms of this magnitude. All nuclear reactions with neutrons of energies less than 1 eV are contemplated for the dose of thermal neutrons (D_{T}). For dosimetric purposes in BNCT, the doses of epithermal neutrons (1 eV < E_n < 10 keV) and fast neutrons (E_n > 10 keV) are grouped into a single dose value, termed only as a fast neutron dose (D_{FE}) (Bisceglie et al., 2000; Raaijmakers et al., 1997). The dosimetric effect of the neutron beam depends on the ^{10}B concentrations in healthy tissue and tumour. In order to obtain the contribution share of the reaction $^{10}\text{B} (n, \alpha) ^7\text{Li}$ in the determination of the total dose, the neutron fluence is modified by flow conversion factors to the kerma and then multiplied by a factor of 10 ppm to represent the concentration 10 μg of ^{10}B per gram of healthy tissue, or a factor of 45.5 ppm, to represent the concentration of 45.5 μg of ^{10}B per gram of tumour tissue. These values are typical of BNCT treatments (Duderstadt, J.J. and Hamilton, 1976). The photon dose component (D_{γ}) is derived from the gamma rays from the interactions of the neutrons with the constituent elements of the tissue. The incident photons originated from the interaction of the neutrons with the irradiated material are not considered in this work for the purposes of dose calculation. The dose limit value in healthy tissue used in this study is the constant value recommended by the protocol of treatments clinical studies from the Brookhaven National Laboratory (Chanana, 1996), which specifies that the dose absorbed by healthy tissue should not exceed 12.5 RBE-Gy at any position in the brain. Table 2 shows the properties of the neutron beam proposed by Goorley et al. (Goorley et al., 2002; IAEA-TECDOC-1223, 2001), used in this study for the different beam diameters.

2.3. Zubal phantom

The reference simulator for the dose calculation was the voxel Zubal phantom (Cui et al., 2019; Evans et al., 2001). The phantoms in voxels are the real representation of the human body and its structure allows us to determine the deposited energy, through the equation of transport of the radiation in the levels of organ or tissue. The Zubal phantom (Evans et al., 2001; Galeano et al., 2014) is a 3-D model of a human head and neck. To create the model, a set of 124 1.4-mm spaced cross-images were made from the head of healthy male volunteers using magnetic resonance imaging. Twenty-two brain structures are identified: amygdala, caudate nucleus, cerebellum, corpus callosum, pale globe, hippocampus, cortex insula, inner capsule, lobar frontal cortex, occipital, parietal lobe, prefrontal and temporal lobe, medulla oblonga, motor cortex, optic nerve, bridge, putamen, pellucid septum, thalamus, uncus and white mass. Seven non-cephalic structures are identified: eyeball, eyes (excluding lens), lacrimal glands, lens, thyroid glands, pituitary gland and cervical spinal cord. Many of the structures identified in the head of the Zubal phantom, including grey matter, adipose tissue, skull skeleton and cartilage, are physiologically irrelevant and

Table 2
Properties of the epithermal beam for different field configurations (Sousa, 2003).

Beam diameter	6 cm	10 cm
Fluency required on the surface of the brain to reach the 12.5 RBE-Gy limit dose in healthy tissue [n/cm ²].	3.86×10^{12}	2.80×10^{12}
Neutron flux required for 1 h of treatment [n/cm ² .s].	10.73×10^8	7.76×10^8

do not need to be considered as a target for calculating the absorbed dose, only its elemental compositions and densities are important for the modelling of radiation transport (Evans et al., 2001). The Zubal simulator is composed of $85 \times 109 \times 120$ voxels, measuring $2.2 \times 2.2 \times 1.4$ mm³.

2.4. Modelling

The neutron source used in the simulation was modelled from a flat, circular geometry with the central beam perpendicular to the surface of the head at 5 cm, according to the experimental geometric configuration of the neutron beam used in BNCT treatments in the MIT-Harvard (Palmer et al., 2002). Two field configurations of different diameters (6 and 10 cm) were studied. The 10 cm diameter beam is commonly used in BNCT treatments (IAEA-TECDOC-1223, 2001; Sousa, 2003). The choice of 6 cm diameter is based on the commitment to evaluate the dose distributions for beams with diameters of the order of tumour volumes (Sousa, 2003). All configurations of simulated beams were monodirectional and evenly distributed in a circular area.

The neutron spectrum used in this work is an idealised beam for BNCT proposed by Goorley et al. (2002). The spectrum is predominantly epithermal (energy distribution $1 \text{ eV} < E_n < 10 \text{ keV}$), contaminated with 1% fast neutrons ($10 \text{ keV} < E_n < 2 \text{ MeV}$) and 10% thermal neutron contamination ($0.001 \text{ eV} < E_n < 1 \text{ eV}$), similar to the idealised beam proposed for clinical use in treatments with BNCT (Bisceglie et al., 2000; Goorley et al., 2002), with each energy distribution obeying the energy distribution $1/E$ and having equal distributions of lethargy.

The fluence conversion factors for the kerma, for photons or neutrons with an energy greater than 0.0253 eV, were obtained from the ICRU Report 46 (White et al., 1992). The fluence conversion factors for the kerma for neutrons with energies less than 0.0253 eV were extrapolated to energies of the order of 10^{-4} eV, using a loglog interpolation, executed by the MCNPX program (MCNP – A General Monte Carlo N-Particle Transport Code, Version 5, Volume I: Overview and Theory, LA-UR-03-1987, 2003). For energies below 1 eV, the movement of the target nucleus is a relevant factor for thermal neutron scattering (Duderstadt, J.J. and Hamilton, 1976). At these low energies, the incident neutron energy is comparable to the thermal energy of the target atom, as well as its chemical bonding energy. Consequently, the thermal movement of the target atom changes the scattering shock section, as well as the resulting energy of the scattered neutron. The treatment of molecular hydrogen bonding in biological materials used was the thermal neutron scattering $S(\alpha, \beta)$ for light water at 300 K (Duderstadt, J.J. and Hamilton, 1976). Another important factor is the correct simulation of the reactions of neutron capture and the subsequent production of photons by the different constituent elements of human tissue. The shock section library used in this work was the ENDF60, which provides sections of continuous and discrete power shocks, using the basic core data of ENDF/B-VI (Rose, 1991), including the corresponding photon production data. The neutron interactions with the ¹⁰B atoms in the tissue were calculated implicitly using the DE/DF command of the MCNP code, which allows rates of nuclear reactions to be calculated to obtain rates integrated in total neutron kerma energy for the nuclear reactions with the ¹⁰B atoms.

The reason for this approximation is due to the fact that for a given patient, it is extremely difficult to measure the concentration of ¹⁰B in the brain tissue in real time and thus the current spatial distribution of

the ¹⁰B atoms not being known in both, pre and post-irradiation, could not be explicitly simulated by MCNP. The ¹⁰B concentration values used are based on biodistribution data obtained during surgery and experiments with positron emission tomography (Palmer et al., 2002; Zamenhof et al., 1990). A total of 50 million histories were used, obtaining a statistical precision of the order of 1%.

3. Results

In this study, we highlight the results obtained in the radiosensitive regions outside the brain and the regions with the highest incidence of tumours, based on studies conducted at the Massachusetts Institute of Technology, USA (Palmer et al., 2002). In this study, it was observed that the region with the highest occurrence of GBM was the parietal lobe, with 13 patients out of a total of 22. Other cases were in the thalamus, temporal lobes, frontal and occipital lobes, cerebellum and bridge regions. In all cases, surgical interventions were performed. The doses administered in these patients ranged from 20.0 to 55.0 RBE-Gy for tumour tissue, and from 0.4 to 16.2 RBE-Gy in healthy tissue (Palmer et al., 2002). Fig. 1, generated by Moritz/MCNP visualization software, illustrates the regions with the highest incidence of cases in the cephalic region. The results will be presented in two stages. The first part describes the dose distributions in the specific tissues of the head and neck region of the Zubal phantom, for neutron beams of 6 and 10 cm in diameter. The second part evaluates the secondary dose contributions in the calculation of the total dose in the regions of higher incidence of tumours and in the non-cephalic regions. Table 3 shows the ability of the neutron beams used to minimise the doses in the normal tissue when the reference dose is released in the tumour, besides minimising the doses in the other tissues radiosensibles of the region of the head and neck.

It is observed that, for the modelling used, the estimated doses in healthy and tumour tissues reach an average difference of 85%. In the tumour tissue, the behaviour observed was the increase in the dose value with the increase of the beam diameter from 6 to 10 cm. Considering that the lowest dose value at which therapeutic advantage can be obtained is of the order of 16.0 RBE-Gy (Sousa, 2003), the use of

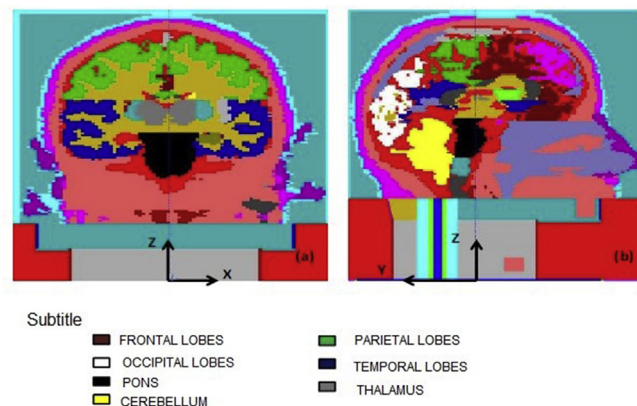


Fig. 1. Locations of the regions with the highest incidence of cancer in the cephalic tissue (Palmer et al., 2002) in the (a) XZ plane and the (b) YZ plane. Image of the Zubal phantom head and neck generated by Moritz/MCNP visualization software (Van Riper and MORITZ Van Riper, 2006).

Table 3

RBE-Gy doses, estimated in tumour and healthy tissues, according to the beam diameters studied. Highlighting regions with higher incidence of tumours (Palmer et al., 2002).

Organs / Tissues	6 cm		10 cm	
	Healthy tissue	Tumour tissue	Healthy tissue	Tumour tissue
AMYGDALA	0.8	5.0	1.5	10.6
CAUDATE NUCLEUS	2.4	18.2	5.5	41.8
CEREBELLUM	0.2	1.2	0.7	3.8
CEREBRAL CORTEX	1.8	14.4	4.5	36.6
CORPUS CALLOSUM	2.1	16.8	5.3	42.6
FRONTAL LOBES	2.4	19.6	5.8	47.6
GLOBUS PALLIDUS	1.9	14.8	4.5	35.8
HIPPOCAMPUS	0.7	4.6	2.1	13.4
INSULA CORTEX	1.1	8.5	3.2	23.8
INTERNAL CAPSULE	2.0	14.9	5.0	39.6
LENTIFORM NUCLEUS	1.7	13.2	4.2	33.3
MEDULLA OBLONGATA	0.3	1.1	0.8	3.4
MOTOR CORTEX	1.1	8.2	3.5	29.4
OCCIPITAL LOBES	0.7	4.9	2.0	15.7
OPTIC NERVE	0.3	2.0	0.7	3.8
PARIETAL LOBES	4.4	37.2	10.5	88.8
PONS	0.6	3.5	1.7	9.7
PREFRONTAL LOBES	1.3	10.4	4.2	33.8
PUTAMEN	1.6	12.5	4.1	32.3
SEPTUM PELLUCIDIUM	2.7	18.9	5.3	44.6
SPINAL CORD	0.1	0.2	0.3	0.7
TEMPORAL LOBES	0.6	3.8	1.6	11.0
THALAMUS	2.0	15.1	4.7	36.9
UNCUS	0.5	3.6	1.6	10.9
WHITE MATTER	1.9	15.7	5.0	40.2
EYEBALLS	0.1	0.6	0.4	2.1
EYES	0.2	0.8	0.5	3.3
LENS	0.1	0.3	0.4	1.5
LACRIMAL GLAND	0.1	0.5	0.5	2.5
PAROTID GLAND	0.1	0.2	0.2	0.6
PITUITARY GLAND	0.9	4.8	2.3	13.4
THYROID	0.0	0.0	0.1	0.2

Table 4

Percentage distribution of individual dose components in healthy tissue in the regions with the highest incidence of tumours, corresponding to the 6 cm diameter beam.

Cephalic regions of higher incidence of tumours	Fast neutrons	Thermal neutrons	Boron	Photons	Total dose (RBE-Gy)
CEREBELLUM	3.62	8.65	32.14	55.60	0.24
FRONTAL LOBES	5.08	15.63	58.70	20.59	2.39
OCCIPITAL LOBES	1.14	14.32	53.19	31.35	0.66
PARIETAL LOBES	5.92	16.15	60.48	17.45	4.41
PONS	9.86	11.33	42.28	36.54	0.57
PREFRONTAL LOBES	1.40	15.55	57.95	25.10	1.28
TEMPORAL LOBES	2.90	12.40	45.86	38.84	0.57
THALAMUS	7.37	14.54	54.12	23.96	1.98

Table 5

Percentage distribution of individual dose components in healthy tissue in the regions with the highest incidence of tumours, corresponding to the 10 cm diameter beam.

Cephalic regions of higher incidence of tumours	Fast neutrons	Thermal neutrons	Boron	Photons	Total dose (RBE-Gy)
CEREBELLUM	5.33	15.46	57.71	21.50	4.52
FRONTAL LOBES	3.67	15.12	56.45	24.76	4.51
OCCIPITAL LOBES	2.67	15.01	55.56	26.76	2.00
PARIETAL LOBES	6.01	16.21	60.67	17.11	10.49
PONS	5.05	10.63	39.81	44.51	1.65
PREFRONTAL LOBES	3.60	15.17	56.72	24.51	4.23
TEMPORAL LOBES	4.22	12.92	47.70	35.16	1.61
THALAMUS	4.82	15.05	55.37	24.76	4.72

the 6 cm diameter beam is feasible for the treatment of tumours located in the parietal lobe, cerebral region where the highest incidence of GBM occurs, as described by Zamenhof and collaborators (Zamenhof et al., 1990). The other regions that can also be treated, because the equivalent doses are above the threshold where therapeutic advantage is obtained (16.0 RBE-Gy), using the beam of 6 cm in diameter, are caldado nucleus, corpus callosum, frontal lobe, parietal lobe and pellucid septum. For the 10 cm diameter, the viability is for the regions of the calyx nucleus, cerebral cortex, corpus callosum, frontal lobe, pale globe, insular cortex, inner capsule, lentiform nucleus, motor cortex, parietal lobe, prefrontal lobe, septum, thalamus and white mass. This study shows that it is possible to achieve dose values in brain tumours compatible with those values present in BNCT treatment without craniotomy. Tables 4 and 5 illustrate the variations of different individual absorbed dose contributions in healthy tissue for the 6 and 10 cm diameter beams, respectively, in the regions of higher incidence of head tumours.

In the regions of the cerebellum and bridge, the percentage of dose due to the photons is greater for the beam with a diameter of 6 cm. This is due to the generation of gamma rays of 2.2 MeV, through the reaction $^1\text{H} (n, \alpha) ^2\text{H}$, to have a greater reach in the tissue. As the neutrons are thermalised and captured as they penetrate the tissue, the dose due to the reaction (n, α) has a lower value for the 6 cm diameter beam, because the cerebellum and the bridge are in a deeper region of the brain, having their values increased to the diameter of 10 cm due to increased thermal neutron fluence, due to the increase in the number of thermalised neutrons outside the projected target volume. For the temporal lobe, occipital and thalamus regions, the largest contribution of the boron dose to the two diameters studied is still present, even though the dose due to the photons has a high percentage, compared to the dose due to the reaction (n, α) , because these tissues are in a more internal region of the head (Fig. 1). In the parietal and frontal

Table 6

Percentage distribution of the individual dose components in the tumour tissue in the regions with the highest incidence of tumours, corresponding to the 6 cm diameter beam.

Cephalic regions of higher incidence of tumours	Fast neutrons	Thermal neutrons	Boron	Photons	Total dose (RBE-Gy)
CEREBELLUM	0.73	1.75	86.30	11.23	1.18
FRONTAL LOBES	0.62	1.90	94.97	2.50	19.65
OCCIPITAL LOBES	0.15	1.90	93.79	4.16	4.95
PARIETAL LOBES	0.70	1.91	95.32	2.07	37.22
PONS	1.59	1.83	90.69	5.89	3.54
PREFRONTAL LOBES	0.17	1.91	94.83	3.09	10.39
TEMPORAL LOBES	0.44	1.87	91.85	5.85	3.76
THALAMUS	0.96	1.90	94.01	3.13	15.13

Table 7

Percentage distribution of the individual dose components in the tumour tissue in the regions with the highest incidence of tumours, corresponding to the 10 cm diameter beam.

Cephalic regions of higher incidence of tumours	Fast neutrons	Thermal neutrons	Boron	Photons	Total dose (RBE-Gy)
CEREBELLUM	0.66	0.66	94.78	2.65	36.58
FRONTAL LOBES	0.46	0.46	94.52	3.12	35.84
OCCIPITAL LOBES	0.34	0.34	94.33	3.42	15.65
PARIETAL LOBES	0.71	0.71	95.35	2.02	88.81
PONS	0.86	0.86	89.79	7.55	9.74
PREFRONTAL LOBES	0.45	0.45	94.57	3.07	33.78
TEMPORAL LOBES	0.61	0.61	92.38	5.12	11.04
THALAMUS	0.62	0.62	94.29	3.17	36.86

lobe regions, a similar behaviour of the dose components for all diameters is observed, because these regions are the most external of the brain (Fig. 1), having a larger value for the dose due to the reaction (n, α). The rapid and thermal neutron doses together account for ~20% of the total dose in the healthy tissue for the two beam diameters studied. In the bridge and thalamus regions, the dose of fast neutrons, due to the $^{14}\text{N}(n, p)^{14}\text{C}$ reaction, decreases as the beam diameter decreases, due to the increased amount of scattered neutrons because of the greater amount of irradiated tissue. For the tumour tissue, Tables 6 and 7 show the variations of the different absorbed dose individual contributions, for the beam diameters of 6 and 10 cm, respectively, in the regions of higher incidence of tumours studied in this study.

As expected, due to the concentration of 45 ppm of ^{10}B , the boron dose has the highest percentage of total dose in the tumour tissue in all regions and for both beams. It is also observed that the contribution of the dose of the fast and thermal neutrons in the total dose presents a percentage below 5%, in all tissues and for the two diameters. The dose of photons was presented as the secondary component that has the highest percentage value. For the cerebellum region, the contribution of the photon dose in the total tumour tissue dose was 11.23% for the 6 cm diameter beam, 8.85% for the 10 cm beam and 6.66%. Other regions that presented a percentage above 5% of photons dose were the bridge with 5.89% for the diameter of 6 cm, 7.55% for the diameter of 10 cm, temporal lobe with 5.85% for the diameter of 6 cm and 5.12% for the diameter of 10 cm. The parietal lobe region presented the lowest percentage of secondary contribution in the total dose for the tumour tissue, totalling 4.66% for the beam diameter of 10 cm, 4.68% for the diameter of 6 cm.

For the 6 cm diameter beam (Table 8), total dose values less than 1.00 RBE-Gy are present in all non-cephalic structures (healthy tissues). It was also found that the highest percentage of dose contribution in all tissues was due to the secondary component of photons. This

Table 8

Total dose and percentage distribution of dose components in non-cephalic tissues to the 6 cm diameter beam.

Radiosisable regions outside the brain	Fast neutrons	Thermal neutrons	Boron	Photons	Total dose (RBE-Gy)
AMYGDALA	7.39	10.87	40.42	41.32	0.83
OPTIC NERVE	1.30	10.25	40.08	48.37	0.34
EYEBALL	1.06	5.83	28.10	65.01	0.14
EYES	1.24	6.72	32.44	59.60	0.16
LENS	1.29	7.73	16.16	74.82	0.09
LACRIMAL GLAND	1.74	10.41	25.52	62.33	0.12
PAROTID GLAND	2.35	6.50	15.82	75.33	0.08
PITUITARY GLAND	5.44	14.44	32.93	47.19	0.94
SPINAL CORD	10.40	3.27	12.11	74.21	0.08
THYROID	8.13	1.01	3.74	87.12	0.03

Table 9

Total dose and percentage distribution of dose components in non-cephalic tissues to the 10 cm diameter beam.

Radiosisable regions outside the brain	Fast neutrons	Thermal neutrons	Boron	Photons	Total dose (RBE-Gy)
AMYGDALA	4.38	13.00	49.61	33.01	1.49
OPTIC NERVE	1.15	6.67	31.38	60.79	0.44
EYEBALL	0.67	8.51	40.60	50.22	0.55
EYES	0.22	14.40	20.30	65.08	0.43
LENS	1.28	14.64	34.77	49.31	0.47
LACRIMAL GLAND	3.61	6.50	16.01	73.87	0.21
PAROTID GLAND	4.49	17.34	38.79	39.37	2.32
PITUITARY GLAND	5.00	2.29	7.97	84.75	0.11
SPINAL CORD	4.38	13.00	49.61	33.01	1.49
THYROID	1.15	6.67	31.38	60.79	0.44

percentage for the photon dose is due to the large number of $^1\text{H}(n, \gamma)^2\text{H}$ reactions that produce photons of 2.2 MeV, which have the great penetration power in biological tissue. With respect to the diameter of 10 cm (Table 9), there was an increase in the values of the total doses in the tissues compared to the diameter of 6 cm, and in the pituitary region reached the value of 2.32 RBE-Gy. The percentage of photon dose decreased with the exception of the spinal cord region. For the boron dose, there was an increase in its percentage in all tissues compared to the diameter of 6 cm. This is due to the increase in thermal neutron fluence in the innermost regions with increasing beam diameter, since the 10 ppm concentration of ^{10}B is the same for all simulated configurations. For the fast neutron component, there was a reduction in the percentage compared to the 6 cm diameter, except in the region of the ocular globe and the parotid. The percentage of the thermal neutron component increased in all regions except for the parotid. The thermal neutron component also showed an increase over the 6 and 10 cm diameters in all tissues. The dose due to the reaction (n, α) presented a higher percentage than the dose of photons in most regions, except in the spinal cord and in the thyroid. This is due to the increase in thermal neutron flux, which increases the occurrence of $^{10}\text{B}(n, \alpha)^7\text{Li}$ reactions in the innermost regions of the head. It is also observed that the higher the percentage of the boron dose the higher the total dose, with the exception of the pituitary region.

4. Conclusions

The choice of beam diameter to use depends on many factors. Among them, the dose should be present in the other radiosensitive regions. According to the optimisation principle, the dose in healthy tissue should be as small as possible (Tauhata, et al., 2013). According to the results obtained for the configurations of neutron beams studied and the comparative analysis with data of treatments in patients found

in the literature, it can be concluded that it is possible to use the beam of 6 cm in diameter for treatment of tumours in the regions of the frontal and parietal lobe. With the neutron beam of 10 cm in diameter it is possible to treat tumours located in the regions of frontal lobe, parietal lobe and thalamus. The parietal lobe region showed the best result with a peak dose of 88.81 RBE-Gy in the tumour tissue for the 10 cm diameter.

In the non-cephalic regions, low dose values (generally less than 1.0 RBE-Gy) were found, indicating that the risks of deterministic effects for these tissues are minimised. The contributions of the thermal, fast neutron and photon components presented different percentages in relation to the total dose in the healthy and tumour tissue, for the simulated beam diameters. Considering the regions with the highest incidence of cases (Palmer et al., 2002), the dose of photons in the healthy tissue presented a larger portion for the cerebellum (diameter of 6 cm and 10 cm) and bridge (diameter 10 cm). However, due to the concentration of 10 ppm of ^{10}B in healthy tissue, the dose due to the reaction (n, α) has the highest percentage in most regions of healthy brain tissue. The summed thermal and fast neutron components total on average 20% of the total dose in healthy brain tissue for all simulated configurations. In tumour tissue, the secondary contribution may reach 15% of the total dose (cerebellar region), with the largest portion being the dose of photons. Therefore, although the dose due to ^{10}B has the greatest contribution to the total dose delivered to the tumour, the secondary contributions exert considerable influence on the determination of the total dose. The undesirable contributions of secondary gamma rays, thermal and fast neutrons can reach 68% of the total dose in healthy brain tissue and 87% of the total dose in the non-cephalic regions. Therefore, this study provides important information regarding doses in the healthy tissues of the head and neck region, which were treated with the BNCT technique.

Author statement

Leandro O. Pereira: Conceptualization, Methodology, Software, Writing - Review & Editing, Data Curation. **Renato P. Freitas:** Software, Writing - Review & Editing, Visualization, Writing - Original Draft, Funding acquisition. **Douglas S. Ferreira:** Software, Writing - Review & Editing, Visualization, Writing - Original Draft, Funding acquisition, Resources. **Valter S. Felix:** Software, Writing - Review & Editing, Visualization. **Elicardo A.S. Gonçalves:** Software, Writing - Review & Editing, Visualization. **André R. Pimenta:** Software, Writing - Review & Editing, Visualization. **Rafael de Sousa Dutra:** Software, Writing - Review & Editing, Visualization. **Ademir Xavier da Silva:** Conceptualization, Software, Writing - Review & Editing, Visualization, Writing - Original Draft, Funding acquisition, Validation, Supervision.

Declaration of competing interest

The authors confirm that there are no known conflicts of interest associated with this publication and there has been no significant financial support for this work that could have influenced its outcome.

Acknowledgments

We thank IFRJ's Pro-rectory of Research, Innovation and Graduate Studies (PROPPI – *Pró-reitoria de Pesquisa, Inovação e Pós-Graduação*) for its financial support grant number 01/2018. The Foundation for Research Support of the State of Rio de Janeiro (FAPERJ - Fundação de Amparo à Pesquisa do Estado do Rio de Janeiro), for their financial support through projects grants numbers E-26/290.066/2018, E-26/

202.672/2018 and E-26.201.867/2018.

References

- Barth, R.F., 2005. Boron neutron capture therapy of cancer: current status and future prospects. *Clin. Cancer Res.* 11, 3987–4002. <https://doi.org/10.1158/1078-0432.CCR-05-0035>.
- Bisceglie, E., Colangelo, P., Colonna, N., Santorelli, P., Variale, V., 2000. On the optimal energy of epithermal neutron beams for BNCT. *Phys. Med. Biol.* 45, 49–58. <https://doi.org/10.1088/0031-9155/45/1/304>.
- Chadwick, J., 1932. The existence of a neutron. *Proc. R. Soc. A Math. Phys. Eng. Sci.* 136, 692–708. <https://doi.org/10.1098/rspa.1932.0112>.
- Chanana, A., 1996. Boron neutron capture therapy of glioblastoma multiforme at the Brookhaven medical research reactor, A phase I/II study. FDA IND 43317 Protocol 4.
- Cui, T., Li, Z., Zhang, S., Wang, Y., Chen, D., Sun, L., 2019. A comparison between GATE and MCNPX for photon dose calculations in radiation protection using a male voxel phantom. *Radiat. Phys. Chem.* 157, 47–53. <https://doi.org/10.1016/j.radphyschem.2018.12.003>.
- Duderstadt, J.J., Hamilton, L.J., 1976. *Nuclear Reactor Analysis*. John Wiley & Sons Ltd., New York.
- Evans, J.F., Blue, T.E., Gupta, N., 2001. Absorbed dose estimates to structures of the brain and head using a high-resolution voxel-based head phantom. *Med. Phys.* 28, 780–786. <https://doi.org/10.1118/1.1354997>.
- Faghihi, F., Khalili, S., 2013. Beam shaping assembly of a D-T neutron source for BNCT and its dosimetry simulation in deeply-seated tumor. *Radiat. Phys. Chem.* 89, 1–13. <https://doi.org/10.1016/j.radphyschem.2013.02.003>.
- Farhad Masoudi, S., Ghiassi, H., Harif, M., Rasouli, F.S., 2018. An electron linac-based system for BNCT of shallow tumors. *Radiat. Phys. Chem.* 148, 106–111. <https://doi.org/10.1016/j.radphyschem.2018.03.001>.
- Galeano, D.C., Cavalcante, F.R., Carvalho, A.B., Hunt, J., 2014. Comparison of conversion coefficients for equivalent dose in terms of air kerma for photons using a male adult voxel simulator in sitting and standing posture with geometry of irradiation antero-posterior. *Radiat. Phys. Chem.* 95, 233–235. <https://doi.org/10.1016/j.radphyschem.2013.05.010>.
- Goorley, J.T., Kiger, W.S., Zamenhof, R.G., 2002. Reference dosimetry calculations for neutron capture therapy with comparison of analytical and voxel models. *Med. Phys.* 29, 145–156. <https://doi.org/10.1118/1.1428758>.
- IAEA-TECDOC-1223, 2001. Current Status of Neutron Capture Therapy. IAEA <https://doi.org/10.1111/j.1558-5646.2008.00544.x>. 2001.
- MCNP, 2003. A General Monte Carlo N-Particle Transport Code, Version 5, Volume I: Overview and Theory, LA-UR-03-1987. Los Alamos National Laboratory, USA.
- Nedunchezian, K., 2016. Boron neutron capture therapy - a literature Review. *J. Clin. Diagn. Res.* <https://doi.org/10.7860/JCDR/2016/19890.9024>.
- Palmer, M.R., Goorley, J.T., Kiger, W.S., Busse, P.M., Riley, K.J., Harling, O.K., Zamenhof, R.G., 2002. Treatment planning and dosimetry for the Harvard-MIT Phase I clinical trial of cranial neutron capture therapy. *Int. J. Radiat. Oncol.* 53, 1361–1379. [https://doi.org/10.1016/S0360-3016\(02\)02862-6](https://doi.org/10.1016/S0360-3016(02)02862-6).
- Raaijmakers, C.P.J., Konijnenberg, M.W., Mijnheer, B.J., 1997. Clinical dosimetry of an epithermal neutron beam for neutron capture therapy: dose distributions under reference conditions. *Int. J. Radiat. Oncol.* 37, 941–951. [https://doi.org/10.1016/S0360-3016\(96\)00623-2](https://doi.org/10.1016/S0360-3016(96)00623-2).
- Rogus, R., 1994. Design and Dosimetry of Epithermal Neutron Beams for Clinical Trials of Boron Neutron Capture Therapy at MITR Reactor. Ph.D. Thesis. Massachusetts Institute of Technology.
- Rogus, R.D., Harling, O.K., Yanch, J.C., 1994. Mixed field dosimetry of epithermal neutron beams for boron neutron capture therapy at the MITR-II research reactor. *Med. Phys.* 21, 1611–1625. <https://doi.org/10.1118/1.597267>.
- Rose, P.F., 1991. ENDF-201: ENDF/B-VI summary documentation. comp, United States. <https://doi.org/10.2172/10132931>.
- Sousa, E.M., 2003. Efeito de interações secundárias no cálculo de dose em tratamentos com captura de nêutrons por boro - BNCT. Dissertação de Mestrado, Instituto de Radioproteção e Dosimetria – IRD, Rio de Janeiro, RJ, Brasil.
- Tauhata, L., Salati, I.P.A., Di Prinzio, R., Di Prinzio, M.A.R.R., 2013. Radioproteção e Dosimetria: Fundamentos - 9ª revisão novembro/2013 - Rio de Janeiro - IRD/CNEN.
- Torres-Sánchez, P., Porras, I., de Saavedra, F.A., Sabariego, M.P., Praena, J., 2019. On the upper limit for the energy of epithermal neutrons for Boron Neutron Capture Therapy. *Radiat. Phys. Chem.* 156, 240–244. <https://doi.org/10.1016/j.radphyschem.2018.11.015>.
- Van Riper, K.A., MORITZ Van Riper, K.A.M., 2006. In: White Rock (Ed.), *Geometry Toll User's Manual: an Interactive Geometry Editor/Viewer for MCNP & MCNPX*, (USA).
- White, D.R., Griffith, R.V., Wilson, I.J., 1992. Report 46. *Int. Comm. Radiat. Units Meas.* <https://doi.org/10.1093/jicru/os24.1.Report46>. os24, NP-NP.
- Zamenhof, R.G., Clement, S.D., Harling, O.K., Brenner, J.F., Wazer, D.E., Madoc-Jones, H., Yanch, J.C., 1990. Monte Carlo based dosimetry and treatment planning for neutron capture therapy of brain tumors. In: *Neutron Beam Design, Development, and Performance for Neutron Capture Therapy*. Springer US, Boston, MA, pp. 283–305. https://doi.org/10.1007/978-1-4684-5802-2_22.